Earthq Eng & Eng Vib (2017) 16: 525-536 **DOI**:10.1007/s11803-017-0406-9

Effect of seismic waves on the hydro-mechanical properties of fractured rock masses

Meysam Lak[1†], Alireza Baghbanan[1‡] and Hamid Hashemolhoseini[2‡]

1. *Department of Mining Engineering, Isfahan University of Technology* (*IUT*)*, Isfahan, Iran*

2. *Department of Civil Engineering, Isfahan University of Technology* (*IUT*)*, Isfahan, Iran*

Abstract: The transmission of seismic waves in a particular region may influence the hydraulic properties of a rock mass, including permeability, which is one of the most important. To determine the effect of a seismic wave on the hydraulic behavior of a fractured rock mass, systematic numerical modeling was conducted. A number of discrete fracture network (DFN) models with a size of 20 m × 20 m were used as geometrical bases, and a discrete element method (DEM) was employed as a numerical simulation tool. Three different boundary conditions without (Type I) and with static (Type II) and dynamic (Type III) loading were performed on the models, and then their permeability was calculated. The results showed that permeability in Type III models was respectively 62.7% and 44.2% higher than in Type I and Type II models. This study indicates that seismic waves can affect deep earth, and, according to the results, seismic waves increase the permeability and change the flow rate patterns in a fractured rock mass.

Keywords: wave transmission; earthquake; dynamic analysis; discrete fracture network; permeability; UDEC

1 Introduction

In rock engineering works, the analysis of the flow of groundwater, oil and gas is as important as the analysis of mechanics in fractured rocks. This analysis must take into account the main components of rock structures: hydraulic conductivity, distributions of pressure and flow rate. Mechanical and hydraulic processes do not occur independently in fractured rocks; they interact with each other. Coupling mechanisms for hydro-mechanical processes include interdependencies between fracture aperture, rock porosity/permeability, fluid pressure and rock stress, among many others (Jing and Stephansson 2007). Consider the example of rock stress. The transmission of seismic waves through a rock mass exerts stress; this stress can influence the rock mass's hydro-mechanical processes. The most significant source of seismic waves is an earthquake. In a short time, an earthquake can influence a rock mass's permeability (a hydraulic property) by causing fluctuations in its amount of stress (a mechanical property).

To shed light on the effect that the transmission of seismic waves has on permeability, we need to deal with the effect of dynamic loading on rock media. Many previous studies have analyzed the effect of earthquake and wave propagation on underground structures in both continuous (Godinho *et al.*, 2013; Cheng *et al.*, 2014;) and discontinuous (Ghazvinian and Rahmatipour, 2005; Li *et al.*, 2015) media. Since the effect of earthquakes on surface structures is more tangible, the literature is full of studies on the dynamic stability analysis of rock slopes (Chuhan *et al.*, 1997; Bhasin and Kaynia, 2004; Wu *et al.*, 2009; Hyodo *et al.*, 2012; Lenti and Martino, 2012; Lin *et al.*, 2012; Zhang *et al.*, 2013; Zhou *et al.*, 2013; Liu *et al.*, 2014; Alfaro *et al.*, 2015; Zhang *et al.*, 2015) and dam structures (Zhang and Wang, 2013). Moreover, a time-domain recursive method to analyze transient wave propagation across rock joints has been evaluated (Li *et al.*, 2012). The study examined the effect of the geometrical properties of parallel joints as well as the mechanical properties of transient wave propagation and transmission/reflection phenomena in the media. However, all of these studies concentrated on the effects of dynamic loading on the mechanical behavior of a rock mass; hydraulic properties were neglected. We believe that the dynamic loading of an earthquake could influence the hydraulic properties of a rock mass, such as its permeability, and that such effects must therefore be scrutinized. The effects of mechanical processes on the hydraulic properties of a rock mass should be considered. For example, top priority should be given to modeling the hydro-mechanics of underground excavations and surrounding areas (Rejeb and Bruel, 2001; Levasseur

Correspondence to: Meysam Lak, Esteghlal sqr., Isfahan University of Technology, Isfahan 84156-83111, Iran
Tel: +98 31 33915128
E-mail: meysam.lak@mi.iut.ac.ir
[†]Msc in Rock Mechanics; [‡]Associate Professor
Received February 23, 2016; **Accepted** August 29, 2016

et al., 2010; Chen *et al.*, 2015; Li and Liu, 2015) and to obtaining the correlation between inflows to tunnels, joint friction angles and joint shear stiffness (Ivars, 2006). A method has been put forward for modeling geo-mechanical couples (Rutqvist *et al.*, 2013).

The direct impact of stress on the hydraulic properties of rock masses has a great deal of importance. In previous studies (e.g., Min *et al.*, 2004a; Baghbanan, 2008; Ma *et al.*, 2013), scale and the effect of stress on the hydro-mechanical properties of rock masses are considered, and the effects of propagating and bending fractures on permeability have been investigated in a deep manner (Latham *et al.*, 2013). Moreover, stress-dependent permeability tensors have also has been studied for jointed rock masses (Min *et al.*, 2004b; Jafari and Babadagli, 2012; He *et al.*, 2013). Also, the relationship between fracture-specific stiffness and fluid flow under different normal stress in a single fracture has been evaluated and reported in the literature (Pyrak-Nolte and Morris, 2000). Recently, a comparison between numerical models of the effect of stress on solute transport in fractured rocks has been accomplished (Zhao *et al.*, 2013). However, although these studies have examined stress effects on the hydraulic properties of rock mass, they have not focused on dynamic stresses; in each case, applied stress was static. Although a study (Derode *et al.,* 2013) has been performed on the coupled seismo-hydromechanical monitoring of inelastic effects on injection-induced fracture permeability, it was only a field-scale study that has not yet been scrutinized for what it suggests about the effects of dynamic loading on the permeability of rock masses. Combined hydraulic and dynamic modeling, with dual simulations of fluid flow and seismic wave propagation, was performed by Vlastos *et al.*, (2006). However, the study numerically examined only the effect of pore pressure changes on seismic wave propagation (i.e., the effects of pore pressures on amplitude, arrival time and frequency content), while the present study aims at assessing a seismic wave's effects on the hydraulic properties of a rock mass.

In this study, we evaluate the effects of an earthquake as dynamic loading on the permeability of a fractured rock mass. Although some researchers assume that seismic waves, such as those generated by an earthquake, cannot affect underground spaces, earthquake waves can influence the rate of inflow to underground excavations. Inflow into underground excavations can affect their short- and long-term stability and thus increase their risk of failure. Since changes of inflow rate are vital in very important projects, earthquake effects should not be ignored. Although an earthquake and its effects are usually adverse, sometimes seismic waves have positive impacts. For example, in the petroleum industry, seismic waves can enhance well productivity (Kouznetsov *et al.*, 1998; Huh, 2006; Mirzaei-Paiaman and Nourani, 2012; Delorme *et al.*, 2013).

In this study, a systematic numerical hydro-mechanical study was performed with three different types of boundary conditions. The current study is in line with studies by Min *et al. (*2004a, 2004b), Blum *et al. (*2005), Baghbanan and Jing (2007, 2008) and Baghbanan (2008), although these studies only considered static loading as a boundary condition. To evaluate the permeability of the fractured crystalline rocks, the discrete fracture network (DFN) approach, a widely used modeling technique, was applied. To adapt discontinuities to real conditions, DFN was used in all models—another difference between our study and other seismo-hydro-mechanical studies. All analyses in this study are based on a discrete element method (DEM) using universal distinct element code (UDEC), which was used in a previous study to facilitate the modeling of wave propagation in rock (Zhao and Chen, 1998).

2 Model description and DFN generation

Fracture systems in rock masses are geometrically complex, leading to a great deal of uncertainty in the quality and quantity of geometric parameter data. These measured data are obtained by field mapping that is performed on the exposed outcrops of limited areas and by borehole logging that results in limited borehole diameters and depths. To alleviate such uncertainty, researchers seek to represent the subsurface fracture system more realistically. The most common method for this—assuming that the geometrical parameters of the fractures are statistically distributed—is stochastic discrete fracture network (DFN) modeling (Baghbanan and Jing, 2007, 2008). Although uncertainties may remain regarding the effect of statistical parameters defined for the geometrical properties of a fracture network in a fractured rock mass (De Dereuzy *et al.*, 2001a, 2001b, 2002; Noetinger and Jarrige, 2012), in the present research, 10 DFN generations have been generated with 20m×20m dimensions based on the field mapping results of the Sellafield area, as utilized by Min *et al.* (2004a, 2004b), Blum *et al.* (2005), Baghbanan and Jing (2007, 2008) and Baghbanan (2008). Thus, random effects were removed through the use of a sufficient number of DFN models. The dimension used here is the representative elementary volume (REV) of permeability, which was approximated and reported in Baghbanan and Jing (2007). By definition, an REV is a certain volume for which a statistical equivalence can be established between the constitutive parameters of the equivalent continuum and the original discontinuum resulting from physical processes (e.g., mechanical deformation and fluid flow transport) (Jing and Stephansson, 2007).

The geometric data are tabulated in Table 1. Four sets of fractures are identified. The orientations of the fracture sets, fracture trace lengths and locations of the fractures follow a Fisher distribution, a truncated power law distribution and a Poisson process respectively (as described in Min *et al.*, 2004a, 2004b; Blum *et al.*, 2005;

Baghbanan, 2008; Baghbanan and Jing, 2007, 2008). Figure 1 shows a sample of these models. Each DFN model contains about 20,000 small rock blocks. Once model geometry was developed, material behavior models needed to be assigned for all of the blocks and discontinuities in the model. In UDEC, there are seven built-in material models for deformable blocks (Itasca, 2000). In reality, when rock media that once contained numerous rock blocks are exposed to a variety of stress conditions, rock blocks will deform. Therefore, in this study, blocks have been assumed to be deformable and a linear elastic constitutive model has been considered for them. In addition to rock block material models, a material model has also been assigned to all discontinuities (as recommended in Itasca, 2000). It should be emphasized that in most previous studies the Coulomb-slip constitutive model has been adopted for joint deformations. It has been common practice to model the behavior of discontinuities by a linear Coulomb relation using the parameters cohesion, c, and friction angle, φ. However, these parameters have major drawbacks, since the relationship between shear strength and normal stress is not linear; it depends upon normal stress (σ_n) and is scale dependent. The application of linear joint models with constant shear and normal stiffness and linear frictional properties is clearly limited when stress changes in large intervals. Since joint shear stiffness (Jk_s) and normal stiffness (Jk_n) increase significantly with normal stress, idealized linear joint behavior models do not adequately predict joint load deformation behavior patterns. Therefore, the nonlinear jointed rock mass behavioral model, such as that derived by Barton and Bandis (1990), is believed to depict a more accurate relationship in rock mass loading, leading to its use in Bhasin and Kaynia (2004) and Blum *et al.* (2005). The Barton-Bandis joint model is a hyperbolic stress-displacement model that accounts for hysteresis due to successive load/unload cycles and hydraulic aperture change based on joint closure and joint roughness in the normal loading stage. During the shear/dilation stage, the model deliberates changes to dilation caused by different normal stress and shear displacement as well as joint damage due to post-peak shear and reduced secondary peak shear upon post-peak shear reversal (Itasca, 2000). There are a few studies in the literature about the effect of cyclic and dynamic shear (Ghosh *et al.*, 1995; Armand, 2000; Jafari *et al.*, 2003, 2004; AminiHosseini *et al.*, 2004; Indraratna *et al.*, 2012) as well as normal loading (Wang *et al.*, 2007; Zhao *et al.*, 2008) on the mechanical properties of rock-joint constitutive models such as Mohr-Coulomb and Barton-Bandis. In general, these studies have found that rock joints display a constant behavior after several successive loading cycles. So far, there is only one reported sensitivity analysis about the effect of cyclic loading on joint constitutive models in UDEC (Ghosh *et al.*, 1995). The results of that analysis show that all of the examined models have some defects in both monotonic and cyclic loadings (Ghosh *et al.*, 1995). However, the Barton-Bandis constitutive model shows good agreement with the experimental results reported in Ghosh *et al.* (1995). Consequently, the Barton-Bandis (BB) non-linear criterion is used here for describing the behavior of joints. The mechanical properties of the intact rock and the joints of our case study, according to the BB model as given in Blum *et al.* (2005), are listed in Table 2.

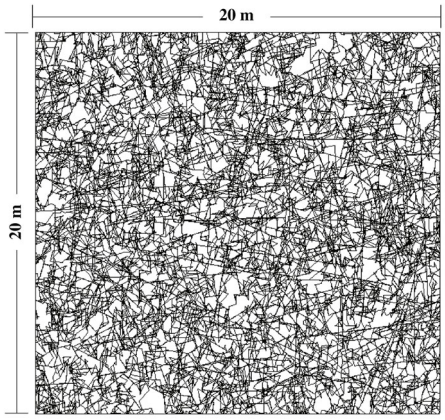

Fig. 1 Sample of the generated DFN models

In the dynamic loading stage, the dynamic mechanical properties of rock are usually greater than their static counterparts. The reported measured values of dynamic Young's modulus, E_d, and Poisson's ratio, ν_d, may be approximated up to 300%, as compared to those values at the static loading condition. Relations between the dynamic values of Young's modulus and Poisson's ratio of the rock and P and S wave velocities are

$$E_d = C_s^2 \rho \left[3\left(C_p/C_s\right)^2 - 4 \right] / \left[\left(C_p/C_s\right)^2 - 1 \right] \quad (1)$$

$$\nu_d = 0.5 \left[\left(C_p/C_s\right)^2 - 2 \right] / \left[\left(C_p/C_s\right)^2 - 1 \right] \quad (2)$$

where E_d and ν_d represent the dynamic values of Young's

Table 1 Geometric parameters of fracture used for DFN generation (Min *et al.*, 2004a, 2004b ; Blum *et al.*, 2005; Baghbanan, 2008; Baghbanan and Jing, 2007, 2008)

Set	Dip/Dip direction	Fisher constant (K)	Fracture density (m^{-2})	Mean trace length (m)
1	8/145	5.9	4.6	0.92
2	88/148	9	4.6	0.92
3	76/21	10	4.6	0.92
4	69/87	10	4.6	0.92

Table 2 Mechanical properties of intact rock and joints (Blum *et al.*, 2005)

Parameters	Symbol	Unit	Value
Intact rock			
Density	ρ	Kg/m^3	2750
Young modulus	E	GPa	84
Poisson ratio	v	-	0.24
Uniaxial compressive strength	UCS	MPa	157
Dynamic Young modulus	E_d	GPa	252
Dynamic Poisson ratio	v_d	-	0.48
BB joints			
Joint roughness coefficient	JRC	-	3.85
Joint wall compressive strength	JCS	MPa	112.2
Normal stiffness	K_n	MPa/m	434000
Shear stiffness	K_s	MPa/m	434000
Residual friction angle	φ_r	°	27.2
Initial aperture	a_i	mm	0.065

modulus and Poisson's ratio respectively. C_p and C_s are P and S wave velocities and ρ is density (Brady, 1993). The magnitude of utilized dynamic values of Young's modulus and Poisson's ratio are reported in Table 2. Note that these dynamic parameters have been used only in the dynamic stage of this study; in other parts of the study, static values have been utilized.

3 Model setup

All analyses in this study are based on a discrete element method (DEM) using Universal Distinct Element Code (UDEC). A discrete element method (DEM) is used to numerically compute motion and effects in a discrete system, including an assemblage of independent units when that has been used to define the problem domain. DEM unit samples may be rock blocks, solid particles of granular materials, structural elements or other individual parts of multibody systems. The formulation of DEM for mechanical analysis is based on the contacts between individual units, their kinematics and their deformation mechanisms (if they are deformable). DEMs appear as one of the most attractive problem-solving approaches in rock engineering and general geomechanics because of their unique advantages in dealing with fractures. The individual units (blocks) in a discrete system move independently according to the force (or stress) restrictions on their boundary surfaces, while other external loads move according to equations of motion. Thus, the rigid body motion of a block can be liberated from other blocks. To account for this, DEMs usually adopt modes for the complete decoupling of rigid body motion and continuous deformation of individual units. The governing equations of DEMS are equations of motion for systems of rigid or deformable units. More precisely, these governing equations are Newton–Euler equations of motion for rigid bodies, Cauchy equations of motion for deformable bodies, the Nervier–Stokes equation for fluid flow through fracture networks and various constitutive equations for a rock matrix and its fractures (Jing and Stephansson, 2007). To directly solve these equations of motion, distinct element programs that incorporate an explicit time-marching scheme can be used. Bodies are assumed to be either rigid or deformable, while contacts are deformable. Deformable bodies are made by subdividing them into elements. UDEC was developed in 1980 (Cundall, 1980; Lemos *et al.*, 1985) to provide two-dimensional modeling of both rigid and deformable blocks divided by discontinuities, enabling either static or dynamic analyses (Itasca, 2000).

In this study, UDEC (version 4.0) was used for static, dynamic and hydraulic modeling. Figure 2 shows the different steps of the general algorithm. According to this algorithm, the geometry of the models was constructed and then the three types of boundary conditions were applied to them. The hydraulic boundary condition was applied directly to Type I models, while in Type II models static loading on the boundary condition was applied first. In another set of numerical simulations (Type III), dynamic loading was assigned and then the numerical hydraulic test was conducted. From now on, Type I, Type II and Type III are abbreviated to T-I, T-II and T-III respectively. As mentioned, all rock blocks in the present study are deformable. In UDEC, deformable blocks are composed of finite difference zones and mechanical changes (e.g., stress/strain) are calculated within each zone (Itasca, 2000).

In this study, given dynamic loading, an element size (i.e., size of finite difference zones) has been considered

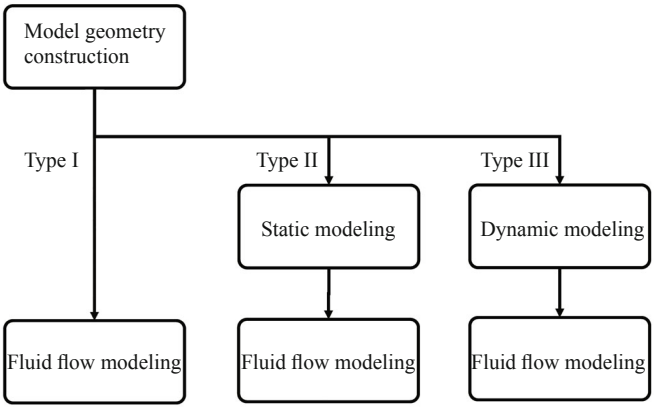

Fig. 2 Problem-solving algorithm

so that it cannot cause numerical distortion. To this end, we obtained the natural frequency of the system as well as the maximum frequency of the input waves. One method for determining natural frequency is to trigger a model to release under its own weight without damping. This causes the system to begin vibrating; because of lack of damping, the vibrations will not stop. The natural frequency can then be obtained by counting the number of oscillations that occur within one second. In our case study, the natural frequency was 71 Hz. Next, a Fast Fourier Transform (FFT) was used to acquire the highest frequency of acceleration for input waves. The maximum frequency of input waves in x-direction was recorded at about 2.87 Hz and in y-direction at 5.46 Hz. The approximately 79,000 zones in each DFN model were then estimated through applying as a constant the rule that the special element size must be smaller than approximately one-tenth to one-eighth of the wavelength. The next subsections explain hydraulic modeling, static loading and dynamic loading separately.

3.1 Hydraulic modeling

The following assumptions were made in the present study's hydraulic modeling. First, the blocks were assumed to be completely impermeable, allowing no flow to pass through them. All of the flow input to the models passed through the cracks, and the flow was a laminar regime. Second, the blocks were assumed to have linear elastic behavior. Third, the fluid was assumed to be water, which is Newtonian and incompressible at a room temperature of 20°C. Moreover, as suggested by Oda *et al.* (1987), if a rock mass is assumed to be an anisotropic continuum porous medium, Darcy's law is validated. Figure 3 illustrates a schematic of the generic boundary conditions for hydraulic modeling. In this closely-packed system, there exists a network of domains, each of which is assumed to be filled with fluid under uniform pressure and in communication with its neighbors through contacts. Flow is governed by the pressure differential between adjacent domains. Flow in planar rock fractures may be idealized by means of a parallel plate model. The analytic solution for laminar viscous flow between parallel plates gives the mean velocity as

$$v = k_{\mathrm{f}} J \tag{3}$$

where J is the hydraulic gradient. The fracture hydraulic conductivity is given by

$$k_{\mathrm{f}} = \frac{a^2 \mathrm{g}}{12\nu} \tag{4}$$

where a is the fracture width, ν is the kinematic viscosity of the fluid and g is the acceleration of gravity. The flow rate per unit width can thus be expressed as

$$q = va = \frac{a^3 \mathrm{g}}{12\nu} J \tag{5}$$

The last equation is usually referred as the "cubic flow law". Since pressure (p) is equal to $g\rho_{\mathrm{w}}h$ (where h is the head), and dynamic viscosity (μ) is equal to $\nu\rho_{\mathrm{w}}$, then Eq. (6) can also be written as

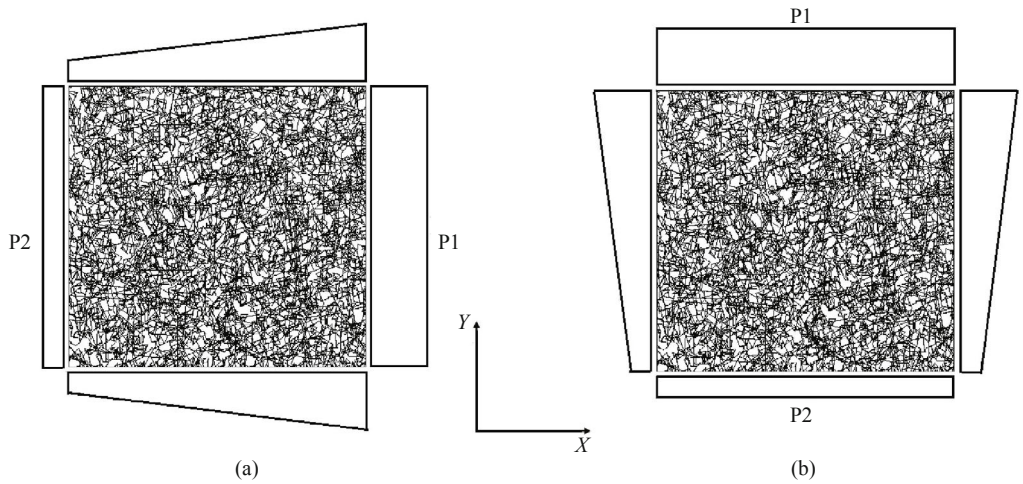

Fig. 3 Hydraulic boundary conditions for calculation of fluid flow and evaluation of permeability of DFN models: (a) in *x*-direction, (b) in y-direction

$$q = -\frac{a^3}{12\mu}\frac{\Delta p}{l} \tag{6}$$

Experiments conducted in Louis (1969) showed that this law is essentially valid for laminar flow in rock joints (Itasca, 2000). The water properties used were ρ_w= 1000 kg/m^3 and μ = 1.0*10^{-3} Pa·s.

In this study, only the final steady-state condition is of interest. Therefore, in light of the foregoing assumptions, and given the appropriate number of joints, fluid flow was modeled on all three types until it reached a steady state. The output flow rate from each boundary was then measured and the permeability matrix calculated in a different direction using Darcy's law perspectives. To get outflow from each bound, all domains on a bound needed to be known and outflow from them added together. The boundary condition shown in Fig. 3a caused fluid to flow in *x*-direction from right to left; it was applied to all three types of model (T-I, T-II and T-III) to obtain k_{xx} and k_{xy} as components of the permeability matrix. Correspondingly, the boundary condition that is shown in Fig. 3b caused fluid to flow in *y*-direction from top to bottom; it was applied to all three types of model to obtain k_{yx} and k_{yy} as components of the permeability matrix. T-I models were introduced during this step without having experienced mechanical loading.

3.2 Static loading

Some previous studies have addressed the effects of static stress on permeability using several types of boundary conditions, as described in Baghbanan and Jing (2008). In this study, upper and lower bounds were fixed in the y-direction and left and right bounds were fixed in the x-direction respectively. Also, 1 MPa of hydrostatic stress was applied to all bounds as a boundary condition. Then, models were entered into hydraulic modeling (T-II). The effects of different static stresses on permeability have been studied elsewhere (Baghbanan, 2008; Baghbanan and Jing, 2008); we have not been focused on that subject.

3.3. Dynamic loading

To develop realistic models and prevent models from damage during dynamic analysis, we adopted the block-in-block (BB) method presented in Blum *et al.* (2005). In this method, the fracture network is located in the center of eight blocks with the uniform material properties of a jointed rock mass. Surrounding blocks are assigned a Young's modulus, E_{mass}, which is representative of the behavior of the equivalent rock mass. The value for intact rock, E_{block}, is used in BB calculations for the central block (Blum *et al.*, 2005). In the present application of this method, modules from the dynamic stage were transformed to their dynamic values using Eq. (1). Figure 4 shows the model constructed using this approach.

Performed following static analysis, dynamic analysis is often very complicated and requires a considerable amount of insight to be interpreted correctly. One issue in dynamic problems is that any unreal boundaries can cause waves to go back into the medium after hitting them. In reality, these waves can be propagated and absorbed infinitely without being returned to the computing medium. Thus, a viscous boundary (i.e., quiet, absorbing) is used in UDEC. The scheme proposed by Lysmer and Kuhlemeyer (1969) involves dashpots attached independently to the boundary in normal and shear directions. The dashpots provide viscous normal and shear tractions given by

$$t_n = -\rho C_p v_n \tag{7}$$

$$t_s = -\rho C_s v_s \tag{8}$$

where v_n and v_s are the normal and shear components of the velocity at the boundary, ρ is the mass density and C_p and C_s are the P and S wave velocities (Itasca, 2000). Here, all model boundaries are absorbing (viscous) (Fig. 5).

Another issue in dynamic problems is that, in the absence of damping, a mechanical system is subjected to driving forces in a continuous mode. To address this in time-domain programs, Rayleigh damping is commonly used to provide damping that is approximately frequency-independent over a restricted range of frequencies. Alternatively, the local damping embodied in UDEC's static solution scheme may be used dynamically, but with a damping coefficient appropriate to wave propagation (Itasca, 2000). Hence, we used local damping with the 0.5 percent coefficient used in past studies (e.g., Kefayati *et al.*, 2011).

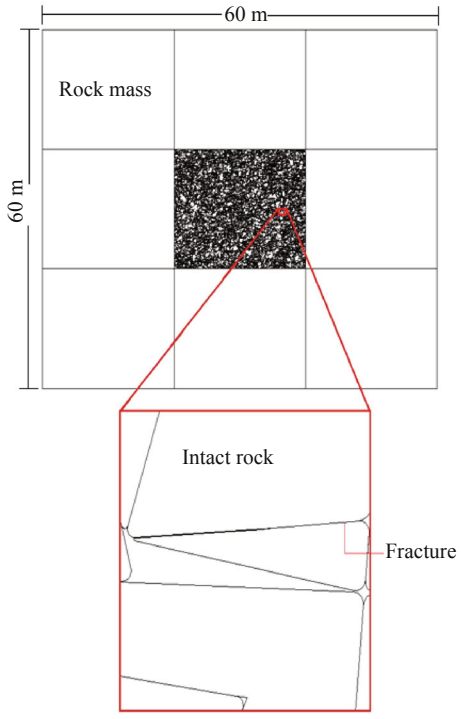

Fig. 4 Model constructed by block-in-block approach

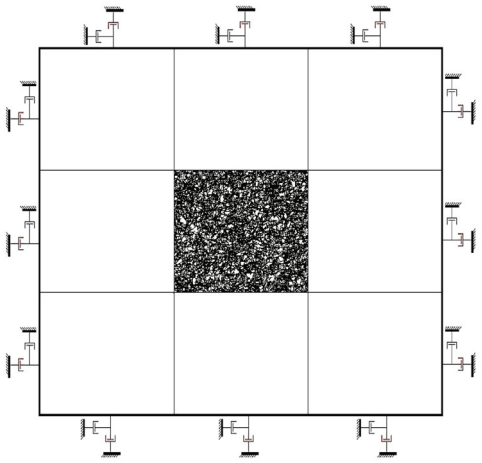

Fig. 5 Boundary conditions in dynamic analysis

Yet another issue in dynamic problems is dynamic input into the system, the most important stage in loading. In UDEC, dynamic input can be applied as velocity history, stress (or pressure) history, or force history. In this study, the Parkfield earthquake, a typical design basis earthquake (DBE), was applied as velocity history to models during dynamic loading. This earthquake, which measured at a 6.1 magnitude on the Richter scale, occurred on June 28, 1966 in California. Figures 6 and 7 illustrate respective components of the acceleration and velocity histories of the Parkfield earthquake,

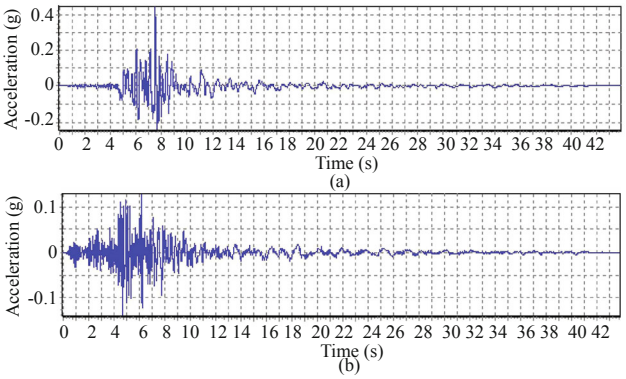

Fig. 6 Acceleration diagram of Parkfield earthquake: (a) in *x*-direction, (b) in *y*-direction (University of California-Berkeley, 2013)

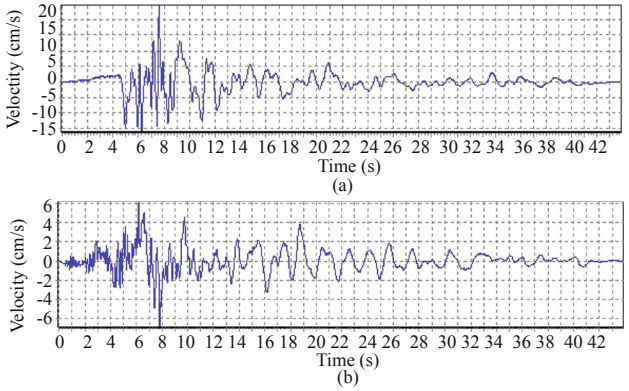

Fig. 7 Input velocity histories: (a) in *x*-direction, (b) in *y*-direction

as applied to models in *x*-and *y*-directions. The peak ground accelerations (PGA) in *x*- and *y*-directions were 0.44g and 0.176g respectively (University of California-Berkeley, 2013). However, UDEC restricts velocity or acceleration input forces from being applied along a boundary that has been set with a quiet boundary condition. To overcome this, a stress boundary condition can be used instead. A velocity wave may be converted to a stress wave using the following formulae

$$\sigma_n = 2\left(\rho C_p\right)v_n \tag{9}$$

$$\sigma_s = 2\left(\rho C_s\right)v_s \tag{10}$$

where σ_n is applied normal stress, σ_s is applied shear stress, ρ is mass density, C_p and C_s are speed of *P* and *S* wave propagation through rock mass, v_n and v_s are input normal and shear particle velocities and C_p and C_s are given by $C_p=\sqrt{(K+4G/3)/\rho}$ and $C_s=\sqrt{G/\rho}$ (Itasca, 2000). The factor of 2 in Eqs. (9) and (10) represents the fact that the applied stress must be doubled to overcome the effect of a viscous boundary (Itasca, 2000). For this reason, we converted the velocity history of the Parkfield earthquake to a stress history and then applied the stress history to the models. After dynamic loading, T-III models were entered into a hydraulic modeling step, following which the permeability of the T-III models was calculated as described in Section 3.1.

4 Results and discussion

As previously stated, on T-I models only fluid-flow modeling was executed. In order to prevent interference on this type from other phenomena, such as the distribution or correlation of fracture aperture and trace length, the initial aperture was set to 65 μm, as had been done in Blum *et al.* (2005). T-II models were developed under hydrostatic boundary conditions and in the next step instantly entered fluid flow modeling. T-III models were exposed under dynamic loading and then entered into fluid flow modeling. In this section, the results from T-I, T-II and T-III models are demonstrated and earthquake effects on rock mass permeability are illustrated. In Fig. 8 permeability matrix components are separated and sorted according to model type. T-I, T-II and T-III models are represented by solid, dashed and dotted lines respectively.

A comparison of the results from T-I and T-III models, as shown in Fig. 8a, demonstrates that dynamic loading increased the value for k_{xx} by 41.4%. This increase in k_{xx} is confirmed by the difference between the means of k_{xx} in T-I and T-III, which were estimated at approximately 3.67×10^{-14} m^2 and 5.19×10^{-14} m^2 respectively. In Fig. 8b, the average values for solid line (T-I) and dotted line (T-III) are approximately 4.25×10^{-13} m^2 and 7.17×10^{-13} m^2 respectively, showing that dynamic loading had an incremental effect of 68.5% on k_{xy} and k_{yx}. In Fig. 8c, the

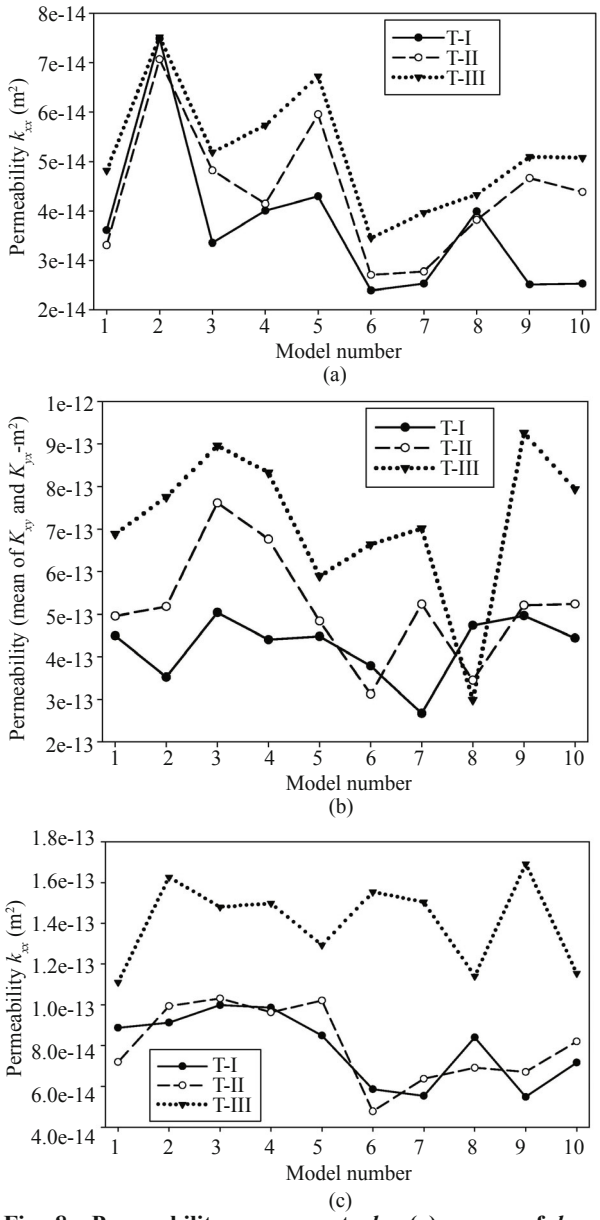

Fig. 8 Permeability components k_{xx} (a), mean of k_{xy} and k_{yx}, (b) and k_{yy} (c) of T-I, T-II and T-III models

mean values of k_{yy} for T-I and T-III are approximately 7.88×10^{-14} m² and 1.4×10^{-13} m² respectively, which confirms an increase of 78.3% in k_{yy} after the occurrence of an earthquake. The reason for the increase in permeability between T-I and T-III is that after dynamic loading was applied to each of the models, the aperture of the joints increased. In T-I models, the aperture had a constant value equal to 65 μm (Fig. 9b). But after applying dynamic loading, the aperture increased until the maximum aperture reached 110 μm (Fig. 9c).

A comparison of the results from T-II and T-III models, as shown in Fig. 8a, demonstrates that the seismic wave increased the value of k_{xx} by 18.9%. This increase in k_{xx} is confirmed by the difference in the mean values of k_{xx} in T-II and T-III, which were approximately 4.36×10^{-14} m² and 5.19×10^{-14} m² respectively. In Fig. 8b - with the exception of Model no. 8–dynamic loading had an average incremental effect of 38.7% on the values of k_{xy} and k_{yx}. The increase in these components' average values ranged from 5.16×10^{-13} m² for T-II to 7.17×10^{-13} m² for T-III, corroborating the authenticity of this result. In Fig. 8c, the mean values of k_{yy} for T-II and T-III varied between approximately 8.02×10^{-14} m² and 1.4×10^{-13} m² respectively. This confirms the increase of 75% in k_{yy} after the occurrence of an earthquake. In other words, dynamic boundary stress caused increased permeability in the study area when compared with static boundary stress. The reason is that the earthquake caused successive movements in the blocks, possibly changing the way they were positioned relative to their previously modeled states. When applied, hydrostatic boundary conditions caused a number of cracks to close in T-II, such as Crack 1 in Fig. 10b.

Figure 10a shows a DFN model with a size of 20 m × 20 m from which we extracted a model with a size of 2 m×2 m (Fig. 10b) in order to show detailed results of aperture changes (thickness of the lines) (Figs. 10c, f), fluid flow rate in *x*-direction (Figs. 10d, g) and y-direction (Figs. 10e, h) and flow path (flow direction) in the specified window in Figs. 10c and 10f in x-direction (Figs. 10i,k) and y-direction (Figs. 10j,l) in T-II and T-III respectively. A comparison of T-II and T-III shows that after applying hydrostatic stress on the boundaries of T-II models, some fractures closed, such as Crack 1 in Fig. 10b (specified by an ellipse). This crack indicates the difference between T-II and T-III in the selected window (Figs. 10c and 10f), while other cracks exist all over the DFN model (Fig. 10a). In Figs. 10c and 10f, a window has been specified which includes one end of Crack 1 and has been shown in Figs. 10i-l. In this way, Figs. 10i and 10j show the flow

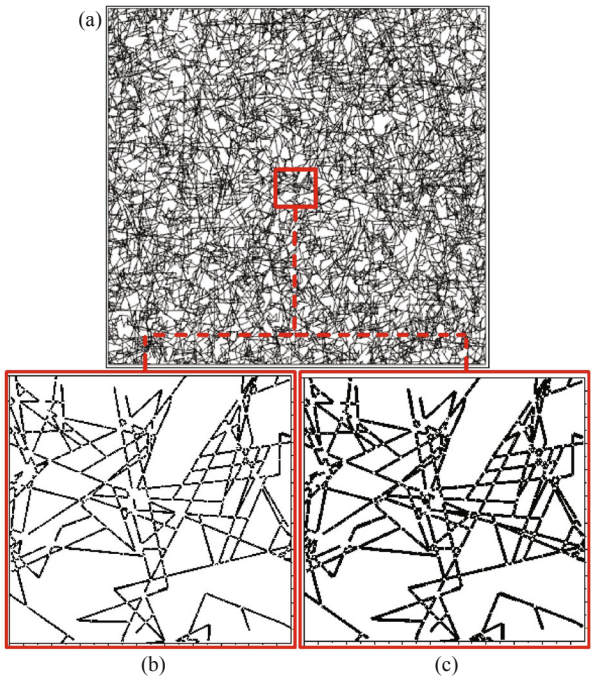

Fig. 9 (a) Aperture changes in 20 m×20 m DFN model for (b) hydraulic (T-I) and (c) dyna-hyromechanic (T-III) conditions. Each line thickness shows 20 μm

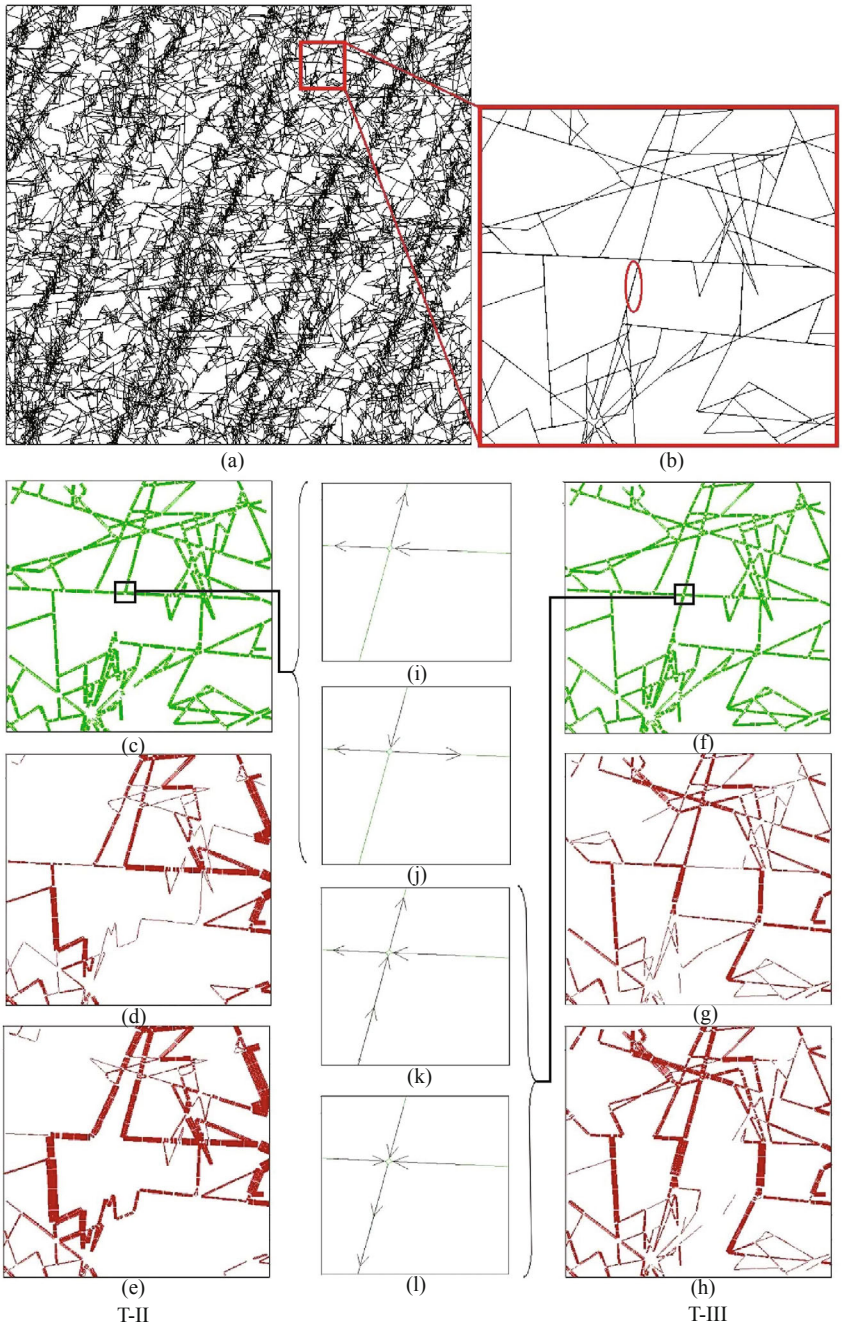

Fig. 10 (a) A DFN model in 20 m × 20 m size. (b) Separated part in 2 m×2 m size. (c, f) Joint aperture in T-II and T-III respectively. Each line thickness shows 20 μm. (d, g) Flow rate in x-direction in T-II and T-III respectively. (e, h) Flow rate in *y*-direction in T-II and T-III respectively. Each line thickness shows 2 × 10^{-7} m^3/s. (i, j) Flow direction in T-II in *x*-direction (i) and *y*-direction (j). (k, l) Flow direction in T-III in x-direction (k) and *y*-direction (l)

path in T-II and Figs. 10k and 10l show the flow path in T-III in *x*- and *y*-directions, respectively. As shown in Figs. 10i (*x*-direction) and 10j (*y*-direction), fluid does not flow in Crack 1 in T-II, while in T-III (Figs. 10k, l) fluid flow passes through it in x- and y-directions. This led to a wider dispersion of flow distribution in T-III (Figs. 10g, h) than in T-II (Fig. 10d, e), and, finally, to greater permeability in T-III than that in T-II. In Fig. 11, the cumulative distribution of flow rates is plotted. As can be seen in this diagram, the cumulative probabilistic density of flow rate in T-III is 10% higher than T-II. A noteworthy point of comparison between Fig. 8a and 8c is that k_{yy} is greater than k_{xx}, as most fractures are

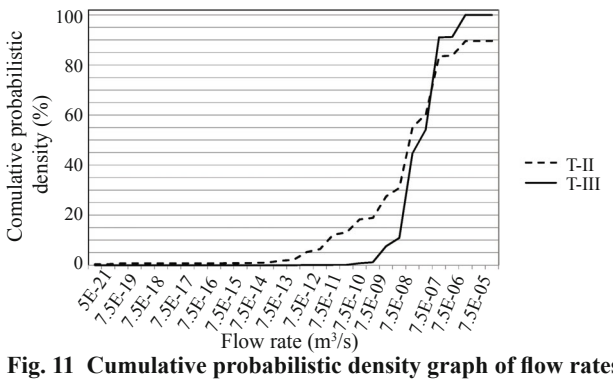

Fig. 11 Cumulative probabilistic density graph of flow rates

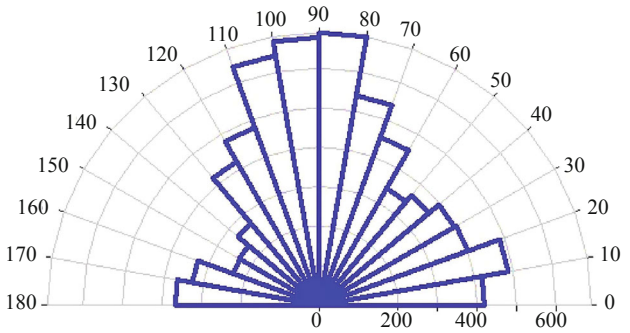

Fig. 12 Joint orientations in DFN models. Radial axis shows joint frequency

oriented sub-vertically. Figure 12 shows a sample of discontinuities in the orientations of the DFN models.

5 Concluding remarks

The effect of an earthquake on the permeability of surrounded rock masses was studied. Despite expectations from previous research, this study finds that seismic waves in deep underground media can have significant effects on the hydro-mechanical properties of a fractured rock mass. Ignoring this phenomenon may put underground openings in great danger. Modeling was conducted in three types with different boundary conditions: non-stress (T-I), static (T-II) and dynamic (T-III). A hydraulic boundary condition was applied to all three types of models, and the following results have been obtained:

- The ability to model seismo-hydromechanics in fractured rock using the DFN technique is one of the main outcomes of this study.
- A comparison of non-stress models (T-I) and dynamic models' (T-III) results showed that permeability increased, on average, to 62.7%. The reason is that the joint aperture increased when the earthquake occurred, so that the maximum joint aperture changed from 65μm to 110μm.
- In T-II models, after hydrostatic boundary conditions were applied, some fractures closed. The earthquake caused successive movement in blocks, possibly changing how they were positioned relative to their previous state and eventually increasing permeability, on average, to 44.2%.
- A comparison of T-II and T-III models' results showed the effects applied stress, so that the computed permeability in the *x*- and *y*-directions for T-II was 4.36×10^{-14} m^2 and 8.02×10^{-14} m^2 respectively and for T-III was 5.19×10^{-14} m^2 and 1.4×10^{-13} m^2 respectively.
- Although all models were surrounded in the deep underground, the loading of a seismic wave changed the apertures and flow patterns, since most fractures experience an open rather than a closed condition.

In this study, the geometrical and mechanical properties of a specific site served only as data sources for generations of more realistic DFN realizations of generic stress-fluid flow simulations that used generated DFN models; they did not serve as a case of site application. The results presented and the conclusions reached therefore have no link to the actual site condition. However, if all the required data were prepared and the same assumptions made, then the approach presented here could be used for other cases. In this study it should be noted that a typical design basis earthquake was used as the seismo-hydromechanical boundary condition, but if a stronger earthquake with a higher frequency were considered, the effects would be more pronounced. The current study is a generic study limited to 2D analysis, since the main object of this study was to highlight the impact of seismic waves on the hydraulic properties of fractured rocks. Therefore, the results and conclusions are also subject to the assumptions made in our modeling, such as constant fracture aperture as well as the specific constitutive model for each individual fracture. A similar study could be carried out in 3D if enough computational source and a fracture constitutive model were available.

References

Alfaro P, Delgado J, García-Tortosa FJ, Giner JJ, Lenti L, López-Casado C, Martino S and Scarascia Mugnozza G (2012), "The Role of Near-field Interaction between Seismic Waves and Slope on the Triggering of a Rockslide at Lorca (SE Spain)," *Natural Hazards and Earth System Sciences*, **12(**3): 631–3643.

Amini-Hosseini K, Pellet F, Jafari MK and Boulon M (2004),"Shear Strength Reduction of Rock Joints Due to Cyclic Loading,"*13th World Conference on Earthquake Engineering*, No. 3070, Vancouver, Canada.

Armand G (2000), "Contribution à la Caracterisation en Laboratoireetà la Modélisationconstitutive du Comportementmécanique des Joints Rocheux, *PhD thesis*, University Joseph Fourier, Grenoble, France. (in French)

Baghbanan A (2008), "Scale and Stress Effects on Hydro-Mechanical Properties of Fractured Rock Masses," *PhD thesis*, Royal Institute of Technology (KTH), Stockholm, Sweden.

Baghbanan A and Jing L (2008), "Stress Effects on Permeability in a Fractured Rock Mass with Correlated Fracture Length and Aperture," *International Journal of Rock Mechanics and Mining Sciences*, **45**: 1320–1334.

Barton N and Bandis SC (1990), "Review of Predictive Capabilities of JRC–JCS Model in Engineering Practice," *International Symposium on Rock Joints*, Loan, Norway.

Bhasin R and Kaynia AM (2004), "Static and Dynamic Simulation of a 700 m High Rock Slope in Western Norway," *Engineering Geology*, **71**: 213–226.

Blum P, Mackay R, Riley MS and Knight JL (2005), "Performance Assessment of a Nuclear Waste Repository: Upscaling Coupled Hydro-mechanical Properties for Far-field Transport Analysis." *International Journal of Rock Mechanics and Mining Sciences*, **42**: 781–792.

Brady BHG (1993), "Dynamic Behavior of Rock," in JA Hudson, editor, *Comprehensive Rock Engineering, Vol. 1: Fundamentals*, Chapter 24, Pergamon Press.

Chen HM, Zhao ZY, Choo LQ and Sun JP (2015), "Rock Cavern Stability Analysis under Different Hydro-geological Conditions Using the Coupled Hydro-mechanical Model," *Rock Mechanics and Rock Engineering*. doi:10.1007/s00603-015-0748-4

Cheng X, Xu W, Yue C, Du X and Dowding CH (2014)."Seismic Response of Fluid-structure Interaction of Undersea Tunnel During Bidirectional Earthquake," *Ocean Engineering*, **75**: 64–70.

Chuhan ZH, Pekau OA, Feng J and Guanglun W (1997), "Application of Distinct Element Method in Dynamic Analysis of High Rock Slopes and Blocky Structures," *Soil Dynamics and Earthquake Engineering*, **16**: 385–394.

Cundall PA (1980). "UDEC—A Generalized Distinct Element Program for Modelling Jointed Rock," Report PCAR-1-80, US Army European Research Office.

De Dreuzy JR, Davy P and Bour O (2001a). "Hydraulic Properties of Two-dimensional Random Fracture Networks Following a Power Law Length Distribution: 1. Effective Connectivity," *Water Resources Research*, **37**(8): 2065–2078.

De Dreuzy JR, Davy P and Bour O (2001b). "Hydraulic Properties of Two-dimensional Random Fracture Networks Following a Power Law Length Distribution: 2. Permeability of Networks Based on Lognormal Distribution of Apertures," *Water Resources Research*, **37**(8): 2079–2095.

De Dreuzy JR, Davy P and Bour O (2002). "Hydraulic Properties of Two dimensional Random Fracture Networks Following Power Law Distributions of Length and Aperture," *Water Resources Research*, **38**(12).

Ghazvinian AH and Rahmatipour S (2005), "Stability of Underground Structures Against the Instantaneous Loading on Ground Surface," *Symposium on Uncertainty Assessment in Dam Engineering*, No. 175S3, Tehran, Iran.

Ghosh A, Hsiung SM and Chowdhury AH (1995), *Seismic Response of Rock Joints and Jointed Rock Mass*, Center for Nuclear Waste Regulatory Analyses, Southwest Research Institute, San Antonio, TX.

Godinho L, Amado-Mendes P, Pereira A and Soares JD (2013), "A Coupled MFS–FEM Model for 2-D Dynamic Soil–structure Interaction in the Frequency Domain," *Computers and Structures*, **129**: 74–85.

Hyodo M, Orense RP, Noda S, Furukawa S and Furui T (2012), "Slope Failures in Residential Land on Valley Fills in Yamamoto Town," *Soils and Foundations*, **52**(5): 975–986.

Indraratna B, Mirzaghorbanali A, Oliveira D and Premadasa WN (2012), "Shear Behaviour of Rock Joints Under Cyclic Loading," *11th Australia-New Zealand Conference on Geomechanics: Ground Engineering in a Changing World*, Australia.

Itasca Consulting Group Inc (2000), *UDEC User's Guide Version 3.0*, Minneapolis, MN.

Ivars M (2006), "Water Inflow into Excavations in Fractured Rock—A Three-dimensional Hydro-mechanical Numerical Study," *International Journal of Rock Mechanics and Mining Sciences*, **43**: 705–725.

Jafari A and Babadagli T (2012), "Estimation of Equivalent Fracture Network Permeability Using Fractal and Statistical Network Properties," *Journal of Petroleum Science and Engineering*, **92-93**: 110–123.

Jing L and Stephansson O (2007), *Fundamentals of Discrete Element Methods for Rock Engineering: Theory and Application*, Elsevier, Amsterdam, Netherlands.

Kefayati S, Baghbanan A, Hashemalhoseini H and Zargari M (2011), "Effect of Block Size on the Seismic Behavior in Fractured Rock Slopes by DFN-DEM Method," *4th Iranian Rock Mechanics Conference*, Tehran, Iran. (in Persian)

Latham JP, Xiang J, Belayneh M, Nick HM, Tsang CF and Blunt MJ (2013), "Modelling Stress-dependent Permeability in Fractured Rock Including Effects of Propagating and Bending Fractures," *International Journal of Rock Mechanics and Mining Sciences*, **57**: 100–112.

Lemos JV, Hart RD and Cundall PA (1985), "A Generalized Distinct Element Program for Modeling Jointed Rock Mass (A Keynote Lecture)," *Proceedings of the International Symposium on Fundamentals of Rock Joints,* Luleå, Sweden, pp. 335–343.

Lenti L and Martino S (2012), "The Interaction of Seismic Waves with Step-like Slopes and its Influence on Landslide Movements," *Engineering Geology*, **126**: 19–36.

Levasseur L, Charlier R, Frieg B and Collin F (2010), "Hydro-mechanical Modeling of the Excavation Damaged Zone Around an Underground Excavation at Mont Terri Rock Laboratory," *International Journal of Rock Mechanics and Mining Sciences*, **43**: 414–425.

Li H, Liu T, Liu Y, Li J, Xia X and Liu B (2015), "Numerical Modeling of Wave Transmission Across Rock Masses with Nonlinear Joints," *Rock Mechanics and Rock Engineering*. doi:10.1007/s00603-015-0766-2

Li JC, Li HB, Ma GW and Zhao J (2012), "A Time-domain Recursive Method to Analyse Transient Wave Propagation Across Rock Joints," *Geophysical Journal International*, **188**: 631–644.

Li L and Liu HH (2015), "EDZ Formation and Associated Hydromechanical Behaviour Around ED-B Tunnel: A Numerical Study Based on a Two-part Hooke's Model (TPHM)," *KSCE Journal of Civil Engineering*, **19**(1): 318–331.

Liu Y, Li H, Xiao K, Li J, Xia X and Liu B (2014), "Seismic Stability Analysis of a Layered Rock Slope,"

Computers and Geotechnics, **55**: 474–481.

Louis C (1969), "A Study of Groundwater Flow in Jointed Rock and Its Influence on the Stability of Rock Masses," Rock Mechanics Research Report, No. 10, Imperial College of Science and Technol.

Ma CY, Liu YT and Wu JL (2013), "Simulated Flow Model of Fractured Anisotropic Media: Permeability and Fracture," *Theoretical and Applied Fracture Mechanics*, **65**: 28–33.

Min KB, Rutqvist J, Tsang CF and Jing L (2004a), "Stress-dependent Permeability of Fractured Rock Masses: A Numerical Study," *International Journal of Rock Mechanics and Mining Sciences*, **41**: 1191–1210.

Min KB, Jing L and Stefansson O (2004b), "Determining the Equivalent Permeability Tensor for Fractured Rock Masses Using a Stochastic REV Approach: Method and Application to the Field Data from Sellafield, UK." *Hydrogeology Journal*, **12**: 497–510.

Oda M, Hatsuyama Y and Ohnishi Y (1987), "Numerical Experiments on Permeability Tensor and Its Application to Jointed Granite at Stripa Mine, Sweden," *Journal of Geophysical Research*, **92**(B8): 8037–8048.

Pyrak-Nolte LJ and Morris JP (2000), "Single Fractures Under Normal Stress: The Relation Between Fracture Specific Stiffness and Fluid Flow," *International Journal of Rock Mechanics and Mining Sciences*, **37**: 245–262.

Rejeb A and Bruel D (2001), "Hydromechanical Effects of Shaft Sinking at the Sellafield Site," *International Journal of Rock Mechanics and Mining Sciences*, **38**: 17–29.

Rutqvist J, Leung C, Hoch A, Wang Y and Wang ZH (2013), "Linked Multicontinuum and Crack Tensor Approach for Modeling of Coupled Geomechanics, Fluid Flow and Transport in Fractured Rock," *Journal of Rock Mechanics and Geotechnical Engineering*, **5**: 18–31.

Vlastos S, LiuE, Main IG, Schoenberg M, Narteau C, Li XY and Maillot B (2006), "Dual Simulations of Fluid Flow and Seismic Wave Propagation in a Fractured Network: Effects of Pore Pressure on Seismic Signature," *Geophysics Journal International*, **166**: 825–838.

Wang WH, Li XB, Zhang YP and Zhuo YJ (2007), "Closure Behavior of Rock Joint under Dynamic Loading," *Journal of Central South University of Technology*, **14**(3): 408–412.

Wu JH, Lin JS and Chen CS (2009), "Dynamic Discrete Analysis of an Earthquake-induced Large-scale Landslide," *International Journal of Rock Mechanics and Mining Sciences*, **46**: 397–407.

Zhang SH and Wang G (2013),"Effects of Near-fault and Far-fault Ground Motions on Nonlinear Dynamic Response and Seismic Damage of Concrete Gravity Dams," *Soil Dynamics and Earthquake Engineering*, **53**: 217–229.

Zhang Y, Chen G, Zheng L, Li Y and Wu J (2013), "Effects of Near-fault Seismic Loadings on Run-out of Large-scale Landslide: A Case Study," *Engineering Geology*, **166**: 216–236.

Zhang Z, Wang T, Wu SH and Tang H (2015), "Rock Toppling Failure Mode Influenced by Local Response to Earthquakes," *Bulletin of Engineering Geology and the Environment.* doi:10.1007/s10064-015-0806-x

Zhao J, Cai JG, Zhao XB and Li HB (2008), "Dynamic Model of Fracture Normal Behaviour and Application to Prediction of Stress Wave Attenuation Across Fractures," *Rock Mechanics Rock Engineering*, **41**(5): 671–693.

Zhao J and Chen SG (1998), "A Study of UDEC Modeling for Blast Wave Propagation in Jointed Rock Masses," *International Journal of Rock Mechanics and Mining Sciences*, **35**(1): 93–99.

Zhao ZH, Rutqvist J, Leung C, Hokr M, Liu Q, Neretnieks I, Hoch A, Havlíček J, Wang Y, Wang ZH, Wu Y and Zimmerman R (2013), "Impact of Stress on Solute Transport in a Fracture Network: A Comparison Study," *Journal of Rock Mechanics and Geotechnical Engineering*, **5**: 110–123.

Zhou JW, Cui P and Yang XG (2013), "Dynamic Process Analysis for the Initiation and Movement of the Donghekou Landslide-debris Flow Triggered by the Wenchuan Earthquake," *Journal of Asian Earth Sciences*, **76**: 70–84.